
ONE-SHOT NEURAL ARCHITECTURE SEARCH WITH NETWORK SIMILARITY DIRECTED INITIALIZATION FOR PATHOLOGICAL IMAGE CLASSIFICATION

Renao Yan

Shenzhen International Graduate School
Tsinghua University
China
yra21@mails.tsinghua.edu

ABSTRACT

Deep learning-based pathological image analysis presents unique challenges due to the practical constraints of network design. Most existing methods apply computer vision models directly to medical tasks, neglecting the distinct characteristics of pathological images. This mismatch often leads to computational inefficiencies, particularly in edge-computing scenarios. To address this, we propose a novel Network Similarity Directed Initialization (NSDI) strategy to improve the stability of neural architecture search (NAS). Furthermore, we introduce domain adaptation into one-shot NAS to better handle variations in staining and semantic scale across pathology datasets. Experiments on the BRACS dataset demonstrate that our method outperforms existing approaches, delivering both superior classification performance and clinically relevant feature localization.

Keywords Neural Architecture Search · Computational Pathology · Network Similarity Directed Initialization · Domain Adaptation

1 Introduction

Breast cancer is among the most prevalent and fatal malignancies affecting women worldwide, posing a major global health burden [1]. Its metastatic nature—commonly spreading to the bones, liver, lungs, and brain—contributes significantly to its incurability [2, 40]. Early detection can dramatically increase the 5-year survival rate to 85%, underscoring the importance of proactive screening [3]. However, manual examination of histological slides remains time-consuming and labor-intensive [4, 5, 42, 44, 45, 46]. With the rising incidence of breast cancer, there is a growing need for automated, efficient diagnostic tools. The digitization of pathology slides has enabled the production of gigapixel images, making large-scale computational analysis feasible.

Deep learning, particularly convolutional neural networks (CNNs), has greatly advanced pathological image analysis, offering improved diagnostic accuracy and efficiency. Nevertheless, designing architectures suited to pathology requires domain-specific considerations. Standard models from natural image domains—such as ResNet or InceptionNet—are often repurposed, but they fail to account for the simpler color distributions and richer hierarchical structures characteristic of pathological images. While researchers typically fine-tune these models using self-supervised or fully supervised approaches, such adaptations often overlook the unique demands of histopathology, resulting in suboptimal outcomes [41]. Moreover, clinical deployment requires not only accuracy but also computational efficiency when processing gigapixel whole slide images (WSIs) in a patch-wise manner on edge devices.

Neural architecture search (NAS), a key technique in automated machine learning (AutoML), has shown promise in generating efficient networks under constraints such as FLOPs or parameter count. Despite its potential, NAS remains underutilized in pathological imaging. Traditional NAS methods like evolutionary algorithms (EA) or Bayesian optimization (BO) often rely on random initialization (RI), which can lead to unstable performance when only a small number of samples are available due to high evaluation cost.

To address this, we propose a two-fold approach. First, we introduce a Network Similarity Directed Initialization (NSDI) strategy to enhance the stability and effectiveness of the search process. Second, we incorporate domain adaptation into one-shot NAS to address distributional shifts caused by varying staining protocols and semantic scales across pathology datasets. The inclusion of domain adaptation loss constrains the supernet to yield more reliable performance estimates, improving evaluation accuracy and overall search quality. Importantly, our method is modular and can be easily integrated into existing NAS pipelines.

This work makes the following key contributions:

- We propose a novel NSDI algorithm that improves the robustness of NAS by reducing redundancy in the initial population, particularly under limited initialization budgets.
- We introduce domain adaptation into one-shot NAS using a Maximum Mean Discrepancy (MMD) loss to mitigate domain shifts in pathological datasets, enabling more reliable architecture evaluation.
- Extensive experiments demonstrate that our method achieves superior classification performance and enhanced search stability compared to existing approaches.

2 Related Works

2.1 Image Classification in Breast Cancer

Most recent studies on breast cancer classification employ weakly supervised techniques, particularly multiple instance learning (MIL), to analyze whole slide image (WSI)-level data. Thandiackal *et al.* proposed ZoomMIL, an end-to-end framework that performs multi-level zooming and outperforms state-of-the-art (SOTA) MIL approaches on the BRIGHT and CAMELYON16 datasets [25]. Zhan *et al.* integrated both region-of-interest (ROI) and WSI-level information for breast tumor classification in the BRIGHT Challenge [28]. Wang *et al.* introduced a weakly supervised method based on cross-slide contrastive learning, which decouples task-agnostic self-supervised feature extraction from task-specific feature refinement and aggregation [29]. Marini *et al.* developed an instance-based MIL model that integrates both strongly and weakly labeled data through a multi-task loss [30]. Wentai *et al.* proposed a MIL pipeline enhanced with transformers for subtype classification [31].

Graph-based approaches have also gained attention. Hou *et al.* designed a spatial-hierarchical graph neural network (GNN) with dynamic structure learning to model spatial dependencies [27]. Pati *et al.* introduced a hierarchical GNN that captures intra- and inter-entity interactions in tissue via entity graphs [32]. Tiard *et al.* proposed a self-supervised method that incorporates stain normalization into a constrained latent space for robust feature learning [26]. Most of these methods focus on WSI-level classification, while patch-level classification remains less explored.

2.2 Neural Architecture Search

NAS typically consists of three components: the search space, the search strategy, and the evaluation method.

2.2.1 Search Space

Zoph *et al.* initially proposed a flexible search space that optimizes the size, stride, and number of kernels in each convolutional layer [6]. Later works such as NASNet [7] introduced modular designs by stacking normal and reduction cells. Zhang *et al.* explored block-based architectures [38]. Liu *et al.* proposed DARTS, which searches over a continuous relaxation of the architecture space using a weight-sharing supernet [8], significantly reducing search cost while achieving competitive results.

Another line of work focuses on optimizing existing architectures through search. ProxylessNAS [9], MDENAS [10], MNasNet [11], FBNet [12], and FBNetV2 [13] all extend MobileNetV2 by adjusting the number, size, and type of convolutional blocks.

2.2.2 Search Strategy

Popular search strategies include random search (RS), Bayesian optimization (BO), evolutionary algorithms (EA), reinforcement learning (RL), and gradient-based methods. Bergstra *et al.* leveraged BO to identify optimal architectures. Zoph *et al.* employed RL to navigate the search space [6], while Real *et al.* demonstrated improved performance using a regularized EA [14]. Liu *et al.* combined parameter sharing with gradient-based search in DARTS to further reduce computational cost [8].

2.2.3 Evaluation Strategy

The standard evaluation approach involves training candidate architectures to convergence and assessing their performance on a validation set. Although accurate, this is computationally expensive. To reduce cost, Klein *et al.* used partial training on subsets of data [15], and Chrabaszcz *et al.* used lower-resolution images [16]. Domhan *et al.* proposed early-stopping strategies based on performance extrapolation from early epochs [17]. Cai *et al.* trained a surrogate model to predict architecture performance from structural encoding [18].

Recent one-shot NAS methods further reduce evaluation cost through weight-sharing supernets, where all candidate architectures share parameters and are evaluated without individual retraining [33].

2.3 NAS Applications in Medical Image Analysis

Despite its success in natural image tasks, NAS has seen limited use in medical imaging. Dong *et al.* introduced a NAS framework for adversarial medical image segmentation [23]. Yan *et al.* proposed MS-NAS, which fuses multi-scale features for cell-level tasks [22]. Tang *et al.* applied a hyperparameter-tuned DARTS framework to computational pathology (CPath), achieving promising results on the ADP dataset [20]. Huang *et al.* developed AdwU-Net, a NAS framework that adapts the depth and width of U-Net for segmentation tasks in the Medical Segmentation Decathlon (MSD) [24]. Eminaga *et al.* proposed PlexusNet, a scalable model family tailored to five clinical classification tasks through structured control of depth, width, and branching [21].

3 Method

We propose a novel neural architecture search (NAS) framework tailored for pathological image analysis, termed Domain Adaptation One-Shot NAS (DAOS). It incorporates a network similarity directed initialization (NSDI) strategy to enhance search stability and introduces domain adaptation into the one-shot NAS paradigm. As shown in Fig. 1, the overall pipeline consists of two main stages: supernet training and architecture search.

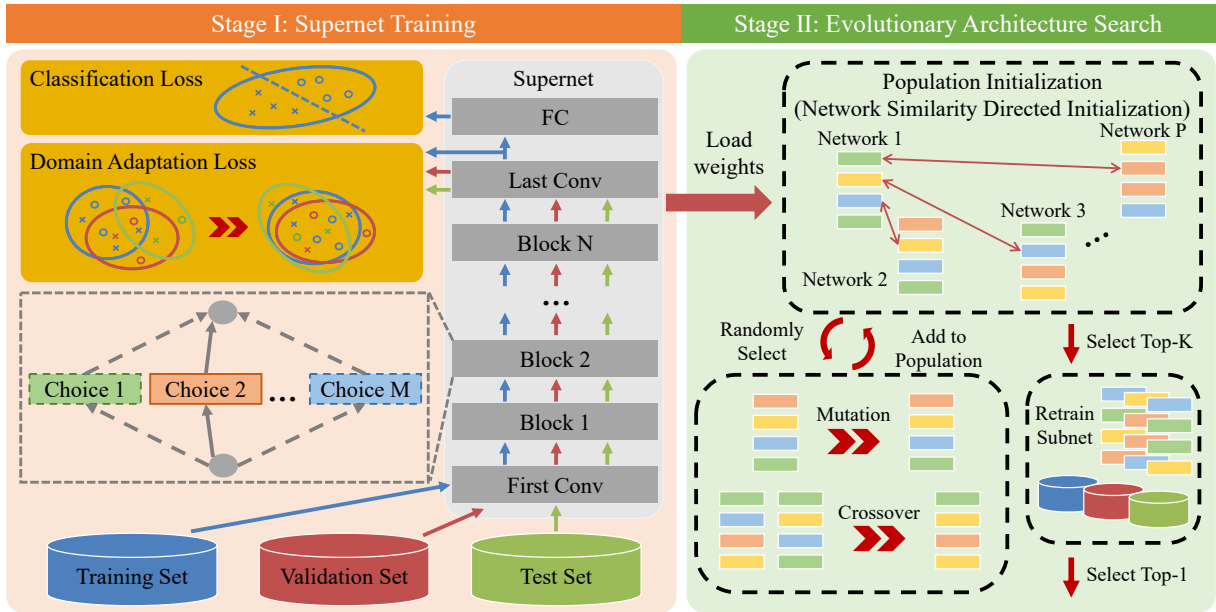


Figure 1: The overview of the proposed domain adaptation one-shot neural architecture search.

The architecture search space \mathcal{A} is modeled as a directed acyclic graph (DAG), where each candidate architecture corresponds to a subgraph $a \in \mathcal{A}$, denoted as $\mathcal{N}_{a,w}$ with weights w . In our design, the search space comprises N layers, each offering M candidate operations, yielding a total of M^N possible architectures.

NAS typically involves training candidate architectures to convergence, then ranking them based on evaluation metrics such as accuracy or F1 score. This process is formalized as:

$$w_a = \underset{w}{\operatorname{argmin}} \mathcal{L}_{\text{train}}(\mathcal{N}_{a,w}), \quad (1)$$

$$a^* = \underset{a \in \mathcal{A}}{\operatorname{argmax}} \operatorname{Metricsval}(\mathcal{N}a, w), \quad (2)$$

where $\mathcal{L}_{\text{train}}(\cdot)$ is the training loss, and $\operatorname{Metricsval}(\cdot)$ denotes validation performance.

3.1 Search Algorithm

We adopt an evolutionary algorithm (EA) for architecture search, using random initialization (RI) to generate the initial population. However, when the population size is small, pseudo-random sampling can result in an imbalanced exploration of the search space. Fig. 2 shows that RI often fails to evenly sample operation choices (e.g., the red box highlights under-represented operators). Although methods like AutoBSS [38] partially address this using clustering-based initialization, they lack consistency.

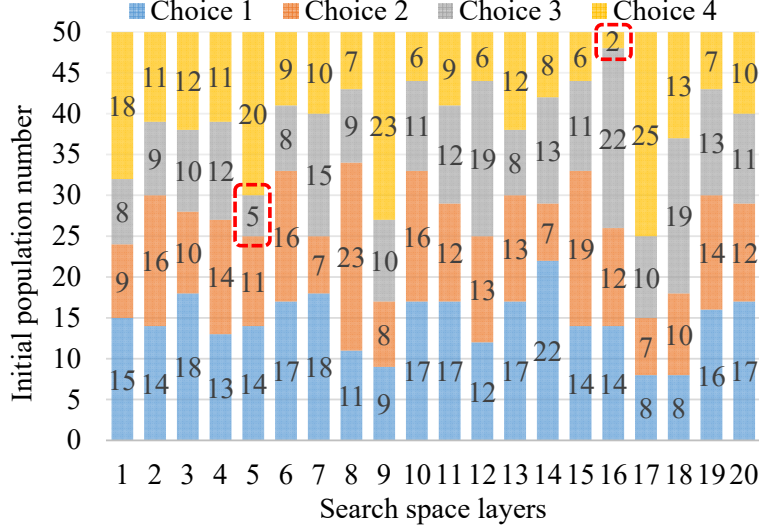


Figure 2: One sample of population initialization under a specific random seed, where the population number is 50, and the search space is a 20-layer network, with four choices in each layer.

To improve population diversity and search stability, we introduce a Network Similarity Directed Initialization (NSDI) method, inspired by force-directed placement (FDP) algorithms [34]. FDP arranges nodes based on repulsive and attractive forces but operates in continuous space, making it unsuitable for discrete search spaces like NAS. Instead, we define a discrete similarity metric to guide initialization.

Specifically, the similarity between two network samples is defined as:

$$\operatorname{SS}(v_i, v_j) \triangleq \sum_{k=0}^N v_{i,k} \odot v_{j,k}, \quad (3)$$

where v_i and v_j are N -dimensional binary vectors encoding architectures a_i and a_j , and \odot denotes the XNOR operation.

We then define the Average Population Similarity (APS) as:

$$\operatorname{APS}(V^P) \triangleq \frac{1}{P} \sum_{i=0}^P \max_{v_j \in V^P, i \neq j} \operatorname{SS}(v_i, v_j), \quad (4)$$

where V^P is the set of P encoded network vectors.

To ensure diversity, we constrain APS under a user-defined threshold $\operatorname{APS}_{\max}$ and increment it adaptively to avoid excessive sampling time. The NSDI process is summarized in Algorithm 1.

3.2 Supernet Training

To avoid retraining every architecture, we adopt a one-shot NAS approach using a shared-weight supernet $\mathcal{N}_{\mathcal{A}, W}$, which spans the entire search space \mathcal{A} with shared weights W . After training, candidate architectures inherit weights from the supernet and are evaluated directly, significantly reducing search cost.

Algorithm 1: Network Similarity Directed Initialization

```

1  Input: population size  $P$ , search depth  $N$ ,  $M$  choices per layer, latency bound  $Lat_{max}$ ,
   similarity threshold  $APs_{max}$ , timeout  $T$ 
2  Output: initialized population  $V$ 
3  While  $\text{len}(V) < P$ :
4       $v = \text{randint}(M, N)$ 
5      if  $\text{len}(V) == 0$ :  $V \leftarrow v$ 
6      else:
7           $SS_{\max} = \max_{u \in V} SS(v, u)$ 
8          if  $SS_{\max} \leq APs_{max}$  and  $\text{Latency}(v) \leq Lat_{max}$ :
9               $V \leftarrow v$ 
10         else:  $t \leftarrow t + 1$ 
11         if  $t > T$ :  $APs_{max} \leftarrow APs_{max} + 1$ ;  $t \leftarrow 0$ 
12  Return population  $V$ 

```

The supernet weights are optimized by minimizing:

$$W_{\mathcal{A}} = \operatorname{argmin} W \mathcal{L}_{\text{train}}(\mathcal{N}_{\mathcal{A}, W}), \quad (5)$$

often approximated by sampling architectures from a prior $\Gamma(\mathcal{A})$:

$$W_{\mathcal{A}} = \operatorname{argmin} W \mathbb{E}_{a \sim \Gamma(\mathcal{A})} [\mathcal{L}_{\text{train}}(\mathcal{N}_{\mathcal{A}, W})], \quad (6)$$

where $\Gamma(\mathcal{A})$ is uniformly sampled under FLOPs constraints.

Given a labeled training set $\mathcal{D}_s = (x_i^s, y_i^s) i = 1^{n_s}$, where $y_i^s \in \mathbb{R}^C$ is a one-hot label, the classification loss is:

$$\mathcal{L}_{\text{cls}}(\mathcal{N}_{\mathcal{A}, W}, \mathcal{D}_s) = \frac{1}{n_s} \sum_{i=1}^{n_s} J(\mathcal{N}_{\mathcal{A}, W_{\mathcal{A}}(a)}(x_i^s), y_i^s), \quad (7)$$

where $J(\cdot, \cdot)$ denotes cross-entropy loss.

3.3 Domain Adaptation with MMD

Weight sharing can lead to performance estimation bias, especially when the training and validation distributions differ (e.g., due to stain variability). To mitigate this, we introduce a domain adaptation loss using Maximum Mean Discrepancy (MMD).

Assume source domain \mathcal{D}_s (labeled training) and target domain $\mathcal{D}_t = x_j^t j = 1^{n_t}$ (unlabeled validation), sampled from different distributions $p \neq q$. MMD quantifies their discrepancy as:

$$d\mathcal{H}(p, q) \triangleq \left| \mathbb{E}_p[\phi(x^s)] - \mathbb{E}_q[\phi(x^t)] \right|^2 \mathcal{H}, \quad (8)$$

where $\phi(\cdot)$ maps samples to a reproducing kernel Hilbert space (RKHS) with kernel $k(x, x') = \langle \phi(x), \phi(x') \rangle$.

An unbiased estimator of MMD is:

$$\hat{d}\mathcal{H}(p, q) = \frac{1}{n_s^2} \sum_{i, j} k(x_i^s, x_j^s) + \frac{1}{n_t^2} \sum_{i, j} k(x_i^t, x_j^t) - \frac{2}{n_s n_t} \sum_{i, j} k(x_i^s, x_j^t). \quad (9)$$

The final training objective combines classification and domain adaptation loss:

$$\mathcal{L}_{\text{train}}(\mathcal{N}_{\mathcal{A}, W}) = \mathcal{L}_{\text{cls}} + \lambda \sum_{\gamma \in q, l} \hat{d}\mathcal{H}(p, \gamma), \quad (10)$$

where λ is a balancing coefficient (set to 0.5 in our experiments).

4 Experiment

4.1 Dataset

Due to the high computational cost of neural architecture search (NAS), we focus our evaluation on a single large-scale dataset—BRACS [36]. The dataset comprises 4,391 breast histological images, scanned using an Aperio AT2 scanner at a resolution of $0.25 \mu\text{m}/\text{pixel}$. All tumor regions-of-interest (TRoIs) are annotated into eight categories: Normal, Benign, Usual Ductal Hyperplasia (UDH), Atypical Ductal Hyperplasia (ADH), Flat Epithelial Atypia (FEA), Ductal Carcinoma In Situ (DCIS), and Invasive. TRoI images vary in spatial resolution, with an average size of 1778×1723 pixels.

4.2 Training Details

We follow the data augmentation protocol introduced in [37], resizing input images to 512×512 pixels. All models are trained using the Adam optimizer ($\beta_1=0.9$, $\beta_2=0.999$, $\epsilon=1\text{e-}8$) to minimize cross-entropy loss. Training is performed on NVIDIA Tesla V100 GPUs using PyTorch v1.7.1 with a batch size of 64.

4.2.1 Search Space

We adopt the one-shot ShuffleNet V2-based search space from [33]. The search space consists of $N = 20$ block layers, each offering $M = 4$ candidate operations. These include Shuffle blocks with kernel sizes of 3×3 , 5×5 , and 7×7 , as well as Xception-style blocks with varying depthwise convolutions. The resulting search space contains 4^{20} possible architectures.

4.2.2 Supernet Training

The supernet is initialized with pre-trained weights from ImageNet [33] and trained for 2000 epochs on BRACS using the single-path strategy as baseline. In the DAOS-A variant, the supernet is further fine-tuned for the final 1000 epochs using a combination of classification and domain adaptation losses. In DAOS-B, the classifier is frozen and the encoder is further fine-tuned for an additional 1000 epochs. The initial learning rate is set to $3\text{e-}4$, and the fine-tuning rate to $1.5\text{e-}4$. A cosine annealing schedule reduces the learning rate to a minimum of $6\text{e-}7$.

4.2.3 Search algorithm

We use evolutionary algorithm with the initialization population $P = 100$, among which the top 50 candidates are selected as the population for further EA-based search. For mutation, a randomly selected candidate mutates its every choice block with a probability of 0.1 to produce a new candidate. For crossover, two randomly selected candidates are crossed to produce a new one. Mutation and crossover are repeated (every 25 operations) for enough new candidates. $\text{FLOPs} \leq 1800\text{M}$ is adopted as the complexity constraint because of the large image size. A total of 1000 candidates are search and the top 10 networks are selected for retraining.

4.2.4 Candidate Retraining

Top-ranked architectures from the search stage inherit weights from the supernet and are then fine-tuned on BRACS for 50 epochs. The learning rate is scheduled from $5\text{e-}6$ to $3\text{e-}4$ using triangular annealing.

4.3 Results and Analysis

4.3.1 NSDI Enhances Search Stability

NAS is inherently a black-box optimization problem, where candidate architectures are encoded as discrete vectors within a combinatorial search space. Due to the high cost of evaluating each network, initializing the population with a representative and diverse set is critical to guiding the search effectively.

As illustrated in Fig.3, evolutionary algorithms (EA) rely on mutation and crossover, which are heavily influenced by the initial population. Poor initialization can trap the search in local optima. To demonstrate this, we compute the average population similarity (APS) for a random-initialized population with $P = 50$, $N = 20$, $M = 4$, and $\text{Lat}_{max} = 1800\text{M}$ FLOPs (Table1). Results show that random initialization yields populations where each architecture is, on average, 50% similar to at least one other sample.

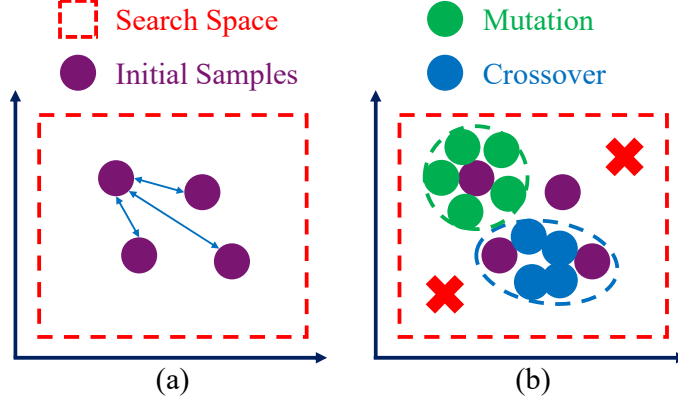


Figure 3: The impact of population initialization on the evolutionary algorithm. (a)Random sampling, (b)mutation and crossover can fall into local optimum.

Table 1: Influence of different population initialization methods on average population similarity

	Random Seed	1	2	3	4	5
RI	APS	10.06	9.94	9.76	9.8	10.22
NSDI	APS	6.98	7.00	7.00	6.98	6.98

By contrast, our NSDI strategy—with $APS_{max} = 6$ and timeout $T = 2 \times 10^5$ —achieves lower APS scores, leading to better diversity, albeit at the cost of more sampling. This trade-off is manageable and can be tuned via T .

Fig.4 compares the F1 score trends across generations for three search strategies. Each method is repeated 10 times.

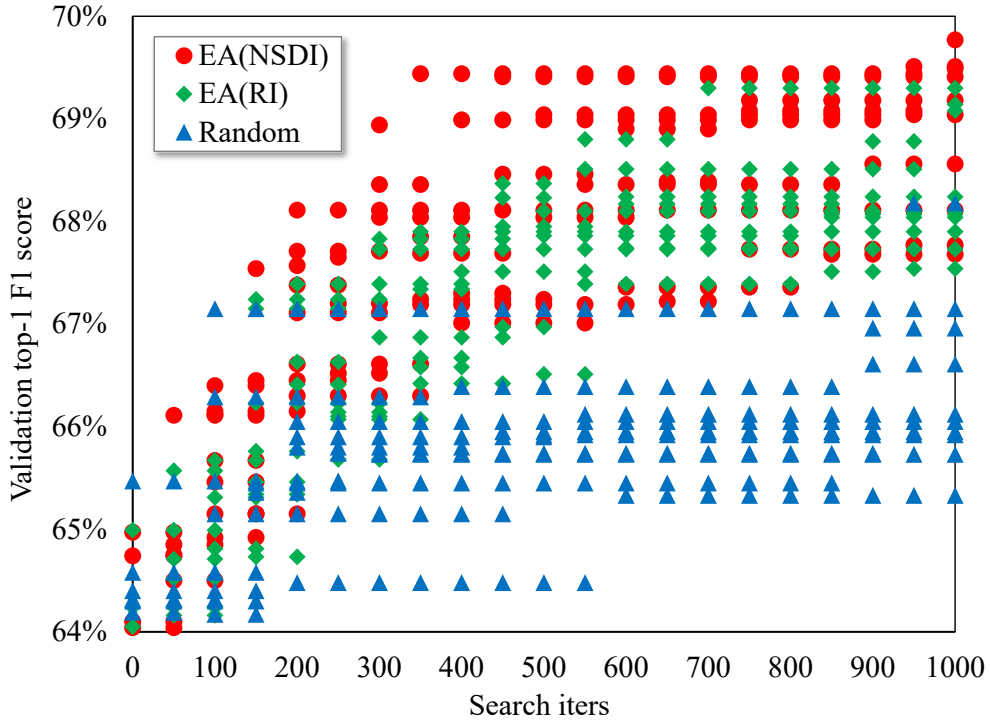


Figure 4: Comparison of random search and evolutionary algorithm with random initialization or network similarity directed initialization.

Table2 summarizes the best performance per trial, showing that EA with NSDI consistently outperforms both random search and EA with random initialization. Despite the time-intensive nature of NAS, our method ensures that the result of each search is consistently close to the global optimum.

Table 2: Best search results on validation set

Seed	Random	EA(RI)	EA(NSDI)
1	65.73	69.66	69.77
2	65.33	68.45	69.04
3	66.61	67.68	68.56
4	68.18	68.92	67.68
5	66.96	67.59	69.41
6	66.05	67.63	69.51
7	67.15	68.62	69.49
8	66.12	67.30	68.09
9	65.95	69.72	69.19
10	65.92	68.13	68.11
Mean	66.40	68.37	68.89
Std	0.79	0.82	0.69

In terms of search cost, DAOS-A matches the training time of SPOS (Table 3). DAOS-B incurs slightly more cost due to the additional fine-tuning of the encoder.

Table 3: Search cost (GPU hours - Ghs)

Method	SPOS	DAOS-A	DAOS-B
Training time (8 GPUs in total)	48 Ghs	48 Ghs	72 Ghs
Search time	16 Ghs	16 Ghs	16 Ghs
Retrain time	8 Ghs	8 Ghs	8 Ghs
Total time	72 Ghs	72 Ghs	96 Ghs

After 1000 search iterations, the top-10 architectures are retrained for evaluation. The best-discovered architecture (F1 = 61.41%) is shown in Fig. 5 and the final performance results are presented in Table 4. Although random search remains a strong baseline, SPOS and EA+NSDI consistently outperform it. Both DAOS-A and DAOS-B further enhance performance and stability, with DAOS-B yielding the most stable outcomes.

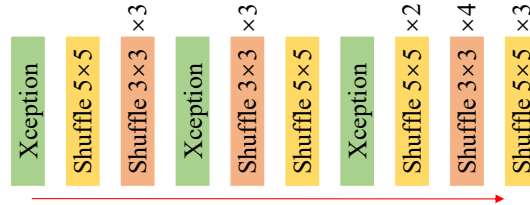


Figure 5: Best architecture searched by DAOS.

4.3.2 Domain Adaptation Improves Supernet Training

We compare three supernet training schemes:

- **Baseline:** 2000 epochs of training using classification loss only.
- **DAOS-A:** Initial 2000 epochs with classification loss, followed by 1000 epochs with added domain adaptation loss.
- **DAOS-B:** Further fine-tuning of the encoder for 1000 epochs while freezing the classifier (after DAOS-A).

Table 4: Top-1 F1 score (%) results on BRACS dataset with different neural architecture search methods (CL: Classification Loss, DAL: Domain Adaptation Loss, FE: Finetune Encoder)

Supernet Training		Random		SPOS		DAOS-A		DAOS-B	
		CL		CL		CL + DAL		CL + DAL + FE	
Search Method		Random		EA		EA		EA	
Initialization Method		Random		Random		NSDI		NSDI	
Random Seed	FLOPs/Params	Top-1 F1	FLOPs/Params	Top-1 F1	FLOPs/Params	Top-1 F1	FLOPs/Params	Top-1 F1	
1	1716M/3.51M	58.96	1727M/3.46M	58.86	1715M/3.20M	58.54	1727M/3.31M	60.08	
2	1718M/3.34M	58.50	1761M/3.22M	57.87	1736M/3.23M	59.33	1673M/3.22M	60.45	
3	1742M/3.34M	58.76	1707M/3.37M	58.17	1713M/3.24M	58.37	1715M/3.28M	58.52	
4	1745M/3.36M	58.60	1708M/3.44M	58.23	1686M/3.22M	59.26	1735M/3.22M	59.56	
5	1758M/3.42M	58.59	1741M/3.38M	57.36	1683M/3.20M	58.98	1764M/3.22M	57.71	
6	1719M/3.33M	58.70	1730M/3.38M	57.76	1716M/3.19M	58.72	1681M/3.21M	59.47	
7	1703M/3.48M	57.89	1738M/3.25M	59.21	1706M/3.21M	59.61	1736M/3.21M	59.56	
8	1763M/3.23M	59.27	1631M/3.32M	59.54	1716M/3.22M	61.41	1653M/3.23M	59.63	
9	1685M/3.37M	57.58	1722M/3.29M	58.58	1689M/3.22M	60.51	1755M/3.32M	59.45	
10	1739M/3.24M	58.29	1742M/3.32M	58.73	1658M/3.21M	58.05	1733M/3.20M	59.06	
Best	1763M/3.23M	59.27	1631M/3.32M	59.54	1716M/3.22M	61.41	1673M/3.22M	60.45	
Average	1729M/3.36M	58.51±0.47	1721M/3.34M	58.43±0.64	1702M/3.21M	59.28±0.97	1717M/3.24M	59.35±0.73	

To assess the effect of domain adaptation, we randomly sample 1000 architectures and evaluate their F1 scores on both validation and test sets. As shown in Fig. 6, the baseline model shows poor correlation between validation and test metrics, meaning a model that performs well on the validation set may generalize poorly. This undermines the reliability of one-shot NAS.

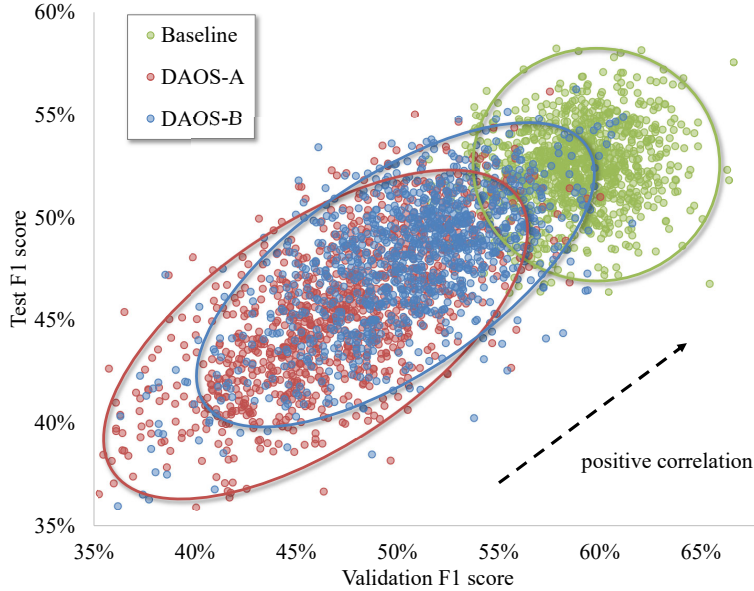


Figure 6: Results of 1000 network evaluation metrics on the validation set and test set. All networks were randomly sampled from the supernet under different training methods. The baseline only uses the classification loss on the training set. DAOS-A uses classification loss and domain adaptation loss. DAOS-B fine-tunes the feature extractor based on DAOS-A by freezing the classifier.

With domain adaptation, both DAOS-A and DAOS-B significantly improve this consistency, yielding a more monotonic relationship between validation and test F1 scores. DAOS-B exhibits the strongest correlation.

Pearson correlation coefficients are computed to quantify this alignment: 0.1794 (Baseline), 0.6985 (DAOS-A), and 0.7096 (DAOS-B). This confirms the effectiveness of our domain adaptation design in stabilizing performance estimation. We further visualize the average feature representations of 1000 networks using t-SNE (Fig. 7). Features

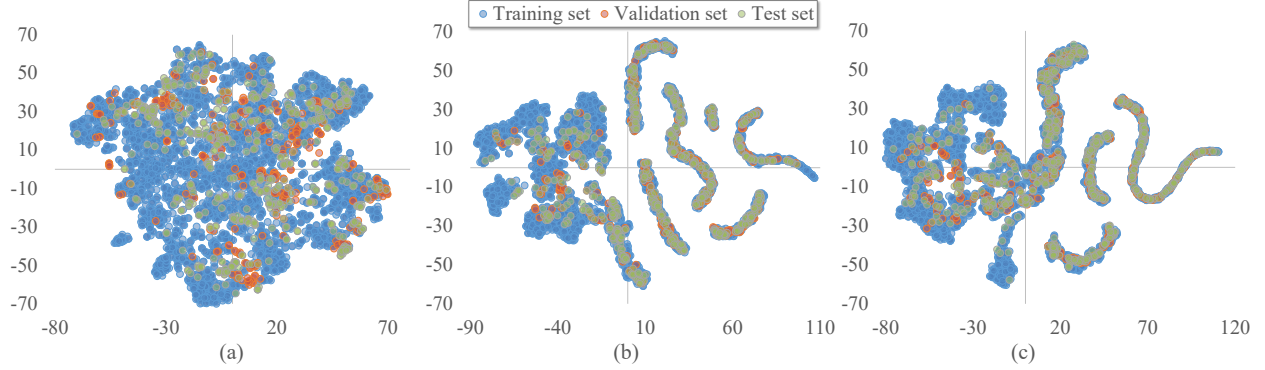


Figure 7: t-SNE of the average supernet features on the training set by different methods. (a) Baseline, (b) DAOS-A, and (c) DAOS-B.

from the baseline supernet are scattered and noisy, whereas those from DAOS-A and DAOS-B exhibit clearer separation and clustering, suggesting improved feature consistency.

4.3.3 DAOS Achieves Superior Performance

To benchmark overall performance, we compare our method against manually designed networks (e.g., ResNet18, InceptionNet V3, MobileNet V2, SqueezeNet variants) and NAS-based models. All models are initialized with ImageNet pre-trained weights and trained on BRACS for 100 epochs with a learning rate of $3e-4$, using the same training configuration as for retraining searched candidates.

Results are reported in Table 5. DAOS-A achieves the highest F1 score among all methods under comparable FLOPs and parameter constraints, demonstrating its efficacy in constrained medical settings.

Table 5: F1 score (%) results on BRACS dataset with different deep learning methods

	Method	FLOPS/Params	F1 score
Manually Designed Networks	ResNet18	9527M/11.18M	60.28
	InceptionNet V3	17629M/21.80M	58.46
	MobileNet V2	1704M/2.23M	57.96
	SqueezeNet V1.0	3989M/0.74M	53.47
	SqueezeNet V1.1	1446M/0.73M	56.56
Neural Architecture Search	Random Search	1731M/3.37M	59.27
	SPOS	1721M/3.34M	59.44
	DAOS-A	1702M/3.21M	61.41
	DAOS-B	1717M/3.24M	60.45

4.3.4 DAOS Improves Pathological Interpretability

Beyond accuracy, interpretability is crucial in clinical applications. We visualize Class Activation Maps (CAMs) [39] for several patches using ResNet18, MobileNet V2, and our method.

As shown in Fig. 8, ResNet18 highlights limited tumor and epithelial regions, while MobileNet V2 attends to irrelevant areas like fat or connective tissue. In contrast, DAOS focuses on a wide range of diagnostically relevant regions—including tumor cells, ducts, and proliferative epithelial structures—better supporting subtype classification. This indicates that our method not only improves accuracy but also enhances clinical relevance and decision support.

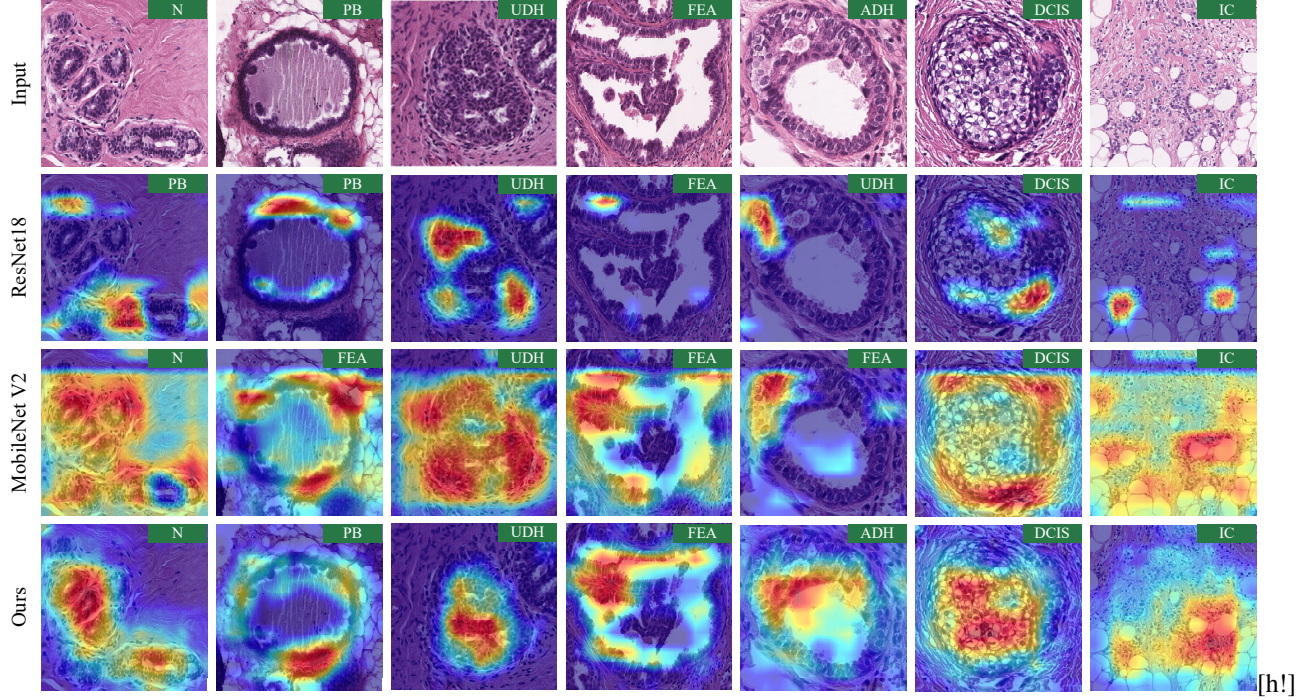


Figure 8: CAMs generated from different methods. The upper left corner of the images show the real labels or predicted labels.

5 Conclusion

In this work, we revisit the one-shot neural architecture search (NAS) paradigm in the context of medical image analysis and identify key limitations when applied to pathological datasets. To address these challenges, we propose a novel framework—Domain Adaptation One-Shot NAS (DAOS)—which integrates a network similarity directed initialization (NSDI) algorithm to improve search stability and introduces domain adaptation to enhance evaluation consistency under domain shifts.

To the best of our knowledge, this is the first work that incorporates domain adaptation into one-shot NAS and explicitly quantifies population diversity during initialization. Our approach achieves strong correlation between validation and test performance, enabling more reliable architecture ranking and selection.

Extensive experiments on the BRACS dataset demonstrate that both DAOS-A and DAOS-B consistently identify high-performing architectures close to the global optimum, outperforming existing baselines in terms of both accuracy and stability. Moreover, the proposed method is highly modular and can be readily extended to other NAS settings, including those based on graph neural networks or Bayesian optimization.

References

- [1] Hyuna Sung, Jacques Ferlay, Rebecca L Siegel, Mathieu Laversanne, Isabelle Soerjomataram, Ahmedin Jemal, and Freddie Bray. Global cancer statistics 2020: Globocan estimates of incidence and mortality worldwide for 36 cancers in 185 countries. *CA: a cancer journal for clinicians*, 71(3):209–249, 2021.
- [2] Yi-Sheng Sun, Zhao Zhao, Zhang-Nv Yang, Fang Xu, Hang-Jing Lu, Zhi-Yong Zhu, Wen Shi, Jianmin Jiang, Ping-Ping Yao, and Han-Ping Zhu. Risk factors and preventions of breast cancer. *International journal of biological sciences*, 13(11):1387, 2017.
- [3] Claudia Allemani, Hannah K Weir, Helena Carreira, et al. Global surveillance of cancer survival 1995–2009: analysis of individual data for 25 676 887 patients from 279 population-based registries in 67 countries (concord-2). *The Lancet*, 385(9972):977–1010, 2015.

- [4] Douglas S Gomes, Simone S Porto, Débora Balabram, and Helenice Gobbi. Inter-observer variability between general pathologists and a specialist in breast pathology in the diagnosis of lobular neoplasia, columnar cell lesions, atypical ductal hyperplasia and ductal carcinoma in situ of the breast. *Diagnostic pathology*, 9:1–9, 2014.
- [5] Joann G. Elmore, Gary M. Longton, Patricia A. Carney, Berta M. Geller, Tracy Onega, Anna N. A. Tosteson, Heidi D. Nelson, Margaret S. Pepe, Kimberly H. Allison, Stuart J. Schnitt, Frances P. O’Malley, and Donald L. Weaver. Diagnostic Concordance Among Pathologists Interpreting Breast Biopsy Specimens. *JAMA*, 313(11):1122–1132, 03 2015.
- [6] Barret Zoph and Quoc V Le. Neural architecture search with reinforcement learning. *arXiv preprint arXiv:1611.01578*, 2016.
- [7] Barret Zoph, Vijay Vasudevan, Jonathon Shlens, and Quoc V Le. Learning transferable architectures for scalable image recognition. In *Proceedings of the IEEE conference on computer vision and pattern recognition*, pages 8697–8710, 2018.
- [8] Hanxiao Liu, Karen Simonyan, and Yiming Yang. Darts: Differentiable architecture search. *arXiv preprint arXiv:1806.09055*, 2018.
- [9] Han Cai, Ligeng Zhu, and Song Han. Proxylessnas: Direct neural architecture search on target task and hardware. *arXiv preprint arXiv:1812.00332*, 2018.
- [10] Xiawu Zheng, Rongrong Ji, Lang Tang, Baochang Zhang, Jianzhuang Liu, and Qi Tian. Multinomial distribution learning for effective neural architecture search. In *Proceedings of the IEEE/CVF International Conference on Computer Vision*, pages 1304–1313, 2019.
- [11] Mingxing Tan, Bo Chen, Ruoming Pang, Vijay Vasudevan, Mark Sandler, Andrew Howard, and Quoc V Le. Mnasnet: Platform-aware neural architecture search for mobile. In *Proceedings of the IEEE/CVF conference on computer vision and pattern recognition*, pages 2820–2828, 2019.
- [12] Bichen Wu, Xiaoliang Dai, Peizhao Zhang, Yanghan Wang, Fei Sun, Yiming Wu, Yuandong Tian, Peter Vajda, Yangqing Jia, and Kurt Keutzer. Fbnet: Hardware-aware efficient convnet design via differentiable neural architecture search. In *Proceedings of the IEEE/CVF Conference on Computer Vision and Pattern Recognition*, pages 10734–10742, 2019.
- [13] Alvin Wan, Xiaoliang Dai, Peizhao Zhang, Zijian He, Yuandong Tian, Saining Xie, Bichen Wu, Matthew Yu, Tao Xu, Kan Chen, et al. Fbnetv2: Differentiable neural architecture search for spatial and channel dimensions. In *Proceedings of the IEEE/CVF Conference on Computer Vision and Pattern Recognition*, pages 12965–12974, 2020.
- [14] Esteban Real, Alok Aggarwal, Yanping Huang, and Quoc V Le. Regularized evolution for image classifier architecture search. In *Proceedings of the aaai conference on artificial intelligence*, volume 33, pages 4780–4789, 2019.
- [15] Aaron Klein, Stefan Falkner, Jost Tobias Springenberg, and Frank Hutter. Learning curve prediction with bayesian neural networks. In *International Conference on Learning Representations*, 2017.
- [16] Patryk Chrabaszcz, Ilya Loshchilov, and Frank Hutter. A downsampled variant of imagenet as an alternative to the cifar datasets. *arXiv preprint arXiv:1707.08819*, 2017.
- [17] Tobias Domhan, Jost Tobias Springenberg, and Frank Hutter. Speeding up automatic hyperparameter optimization of deep neural networks by extrapolation of learning curves. In *Twenty-fourth international joint conference on artificial intelligence*, 2015.
- [18] Han Cai, Tianyao Chen, Weinan Zhang, Yong Yu, and Jun Wang. Efficient architecture search by network transformation. In *Proceedings of the AAAI Conference on Artificial Intelligence*, volume 32, 2018.
- [19] Yu Weng, Tianbao Zhou, Yujie Li, and Xiaoyu Qiu. Nas-unet: Neural architecture search for medical image segmentation. *IEEE access*, 7:44247–44257, 2019.
- [20] Sheyang Tang, Mahdi S Hosseini, Lina Chen, Sonal Varma, Corwyn Rowsell, Savvas Damaskinos, Konstantinos N Plataniotis, and Zhou Wang. Probeable darts with application to computational pathology. In *Proceedings of the IEEE/CVF International Conference on Computer Vision*, pages 572–581, 2021.
- [21] Okyaz Eminaga, Mahmoud Abbas, Jeanne Shen, Mark Laurie, James D Brooks, Joseph C Liao, and Daniel L Rubin. Plexusnet: A neural network architectural concept for medical image classification. *Computers in Biology and Medicine*, page 106594, 2023.
- [22] Xingang Yan, Weiwen Jiang, Yiyu Shi, and Cheng Zhuo. Ms-nas: Multi-scale neural architecture search for medical image segmentation. In *Medical Image Computing and Computer Assisted Intervention–MICCAI 2020: 23rd International Conference, Lima, Peru, October 4–8, 2020, Proceedings, Part I 23*, pages 388–397. Springer, 2020.

- [23] Nanqing Dong, Min Xu, Xiaodan Liang, Yiliang Jiang, Wei Dai, and Eric Xing. Neural architecture search for adversarial medical image segmentation. In *Medical Image Computing and Computer Assisted Intervention–MICCAI 2019: 22nd International Conference, Shenzhen, China, October 13–17, 2019, Proceedings, Part VI* 22, pages 828–836. Springer, 2019.
- [24] Ziyang Huang, Zehua Wang, Zhikai Yang, and Lixu Gu. Adwu-net: adaptive depth and width u-net for medical image segmentation by differentiable neural architecture search. In *International Conference on Medical Imaging with Deep Learning*, pages 576–589. PMLR, 2022.
- [25] Kevin Thandiackal, Boqi Chen, Pushpak Pati, Guillaume Jaume, Drew FK Williamson, Maria Gabrani, and Orcun Goksel. Differentiable zooming for multiple instance learning on whole-slide images. In *Computer Vision–ECCV 2022: 17th European Conference, Tel Aviv, Israel, October 23–27, 2022, Proceedings, Part XXI*, pages 699–715. Springer, 2022.
- [26] Alexandre Tiard, Alex Wong, David Joon Ho, Yangchao Wu, Eliram Nof, Stefano Soatto, and Saad Nadeem. Stain-invariant self supervised learning for histopathology image analysis. *arXiv preprint arXiv:2211.07590*, 2022.
- [27] Wentai Hou, Helong Huang, Qiong Peng, Rongshan Yu, Lequan Yu, and Liansheng Wang. Spatial-hierarchical graph neural network with dynamic structure learning for histological image classification. In *Medical Image Computing and Computer Assisted Intervention–MICCAI 2022: 25th International Conference, Singapore, September 18–22, 2022, Proceedings, Part II*, pages 181–191. Springer, 2022.
- [28] Yangen Zhan, Hao Bian, Yang Chen, Xiu Li, and Yongbing Zhang. Breast tumor image classification in bright challenge via multiple instance learning and deep transformers. In *2022 IEEE International Symposium on Biomedical Imaging Challenges (ISBIC)*, pages 1–5. IEEE, 2022.
- [29] Xiyue Wang, Jinxi Xiang, Jun Zhang, Sen Yang, Zhongyi Yang, Ming-Hui Wang, Jing Zhang, Yang Wei, Junzhou Huang, and Xiao Han. Scl-wc: Cross-slide contrastive learning for weakly-supervised whole-slide image classification. In *Advances in Neural Information Processing Systems*.
- [30] Niccolò Marini, Marek Wodzinski, Manfredo Atzori, and Henning Müller. A multi-task multiple instance learning algorithm to analyze large whole slide images from bright challenge 2022. In *2022 IEEE International Symposium on Biomedical Imaging Challenges (ISBIC)*, pages 1–4. IEEE, 2022.
- [31] Feng Wentai, Kuang Jinbo, Ji Zheng, and Xu Shuoyu. Multiple-instance learning with efficient transformer for breast tumor image classification in bright challenge. In *2022 IEEE International Symposium on Biomedical Imaging Challenges (ISBIC)*, pages 1–5. IEEE, 2022.
- [32] Pushpak Pati, Guillaume Jaume, Antonio Foncubierto-Rodriguez, Florinda Feroce, Anna Maria Anniciello, Giosue Scognamiglio, Nadia Brancati, Maryse Fiche, Estelle Dubruc, Daniel Riccio, et al. Hierarchical graph representations in digital pathology. *Medical image analysis*, 75:102264, 2022.
- [33] Zichao Guo, Xiangyu Zhang, Haoyuan Mu, Wen Heng, Zechun Liu, Yichen Wei, and Jian Sun. Single path one-shot neural architecture search with uniform sampling. In *Computer Vision–ECCV 2020: 16th European Conference, Glasgow, UK, August 23–28, 2020, Proceedings, Part XVI* 16, pages 544–560. Springer, 2020.
- [34] Thomas MJ Fruchterman and Edward M Reingold. Graph drawing by force-directed placement. *Software: Practice and experience*, 21(11):1129–1164, 1991.
- [35] Arthur Gretton, Karsten M Borgwardt, Malte J Rasch, Bernhard Schölkopf, and Alexander Smola. A kernel two-sample test. *The Journal of Machine Learning Research*, 13(1):723–773, 2012.
- [36] Nadia Brancati, Anna Maria Anniciello, Pushpak Pati, Daniel Riccio, Giosuè Scognamiglio, Guillaume Jaume, Giuseppe De Pietro, Maurizio Di Bonito, Antonio Foncubierto, Gerardo Botti, et al. Bracs: A dataset for breast carcinoma subtyping in h&e histology images. *Database*, 2022, 2022.
- [37] Hugo Touvron, Matthieu Cord, Matthijs Douze, Francisco Massa, Alexandre Sablayrolles, and Herve Jegou. Training data-efficient image transformers & distillation through attention. In *International Conference on Machine Learning*, volume 139, pages 10347–10357, July 2021.
- [38] Yikang Zhang, Jian Zhang, and Zhao Zhong. Autobss: An efficient algorithm for block stacking style search. *Advances in Neural Information Processing Systems*, 33:10259–10270, 2020.
- [39] Bolei Zhou, Aditya Khosla, Agata Lapedriza, Aude Oliva, and Antonio Torralba. Learning deep features for discriminative localization. In *Proceedings of the IEEE conference on computer vision and pattern recognition*, pages 2921–2929, 2016.
- [40] Lianghui Zhu, Huijuan Shi, Huiting Wei, Chengjiang Wang, Shanshan Shi, Fenfen Zhang, Renao Yan, Yiqing Liu, Tingting He, Liyuan Wang, et al. An accurate prediction of the origin for bone metastatic cancer using deep learning on digital pathological images. *EBioMedicine*, 87, 2023.

- [41] Renao Yan, Qiming He, Yiqing Liu, Peng Ye, Lianghui Zhu, Shanshan Shi, Jizhou Gou, Yonghong He, Tian Guan, and Guangde Zhou. Unpaired virtual histological staining using prior-guided generative adversarial networks. *Computerized Medical Imaging and Graphics*, 105:102185, 2023.
- [42] Renao Yan, Qiehe Sun, Cheng Jin, Yiqing Liu, Yonghong He, Tian Guan, and Hao Chen. Shapley values-enabled progressive pseudo bag augmentation for whole-slide image classification. *IEEE Transactions on Medical Imaging*, 2024.
- [43] Xinrui Chen, Yizhi Wang, Renao Yan, Yiqing Liu, Tian Guan, and Yonghong He. Texq: zero-shot network quantization with texture feature distribution calibration. *Advances in Neural Information Processing Systems*, 36:274–287, 2023.
- [44] Mingxi Ouyang, Yuqiu Fu, Renao Yan, ShanShan Shi, Xitong Ling, Lianghui Zhu, Yonghong He, and Tian Guan. Mergeup-augmented semi-weakly supervised learning for wsi classification. *arXiv preprint arXiv:2408.12825*, 2024.
- [45] Xuenian Wang, Shanshan Shi, Renao Yan, Qiehe Sun, Lianghui Zhu, Tian Guan, and Yonghong He. Task-oriented embedding counts: Heuristic clustering-driven feature fine-tuning for whole slide image classification. *arXiv preprint arXiv:2406.00672*, 2024.
- [46] Lianghui Zhu, Renao Yan, Tian Guan, Fenfen Zhang, Linlang Guo, Qiming He, Shanshan Shi, Huijuan Shi, Yonghong He, and Anjia Han. Hierarchically optimized multiple instance learning with multi-magnification pathological images for cerebral tumor diagnosis. *IEEE Journal of Biomedical and Health Informatics*, 2025.